Machine-enhanced *CP*-asymmetries in the electroweak sector

Noah Clarke Hall,[1] Isaac Criddle,[1] Archie Crossland,[1] Christoph Englert,[2,*] Patrick Forbes,[1] Robert Hankache,[1] and Andrew D. Pilkington[1,†]

[1]*Department of Physics and Astronomy, University of Manchester, Manchester M13 9PL, United Kingdom*
[2]*School of Physics and Astronomy, University of Glasgow, Glasgow G12 8QQ, United Kingdom*

(Received 26 September 2022; accepted 2 January 2023; published 18 January 2023)

The violation of charge conjugation (C) and parity (P) symmetries are a requirement for the observed dominance of matter over antimatter in the Universe. As an established effect of beyond the Standard Model physics, this could point towards additional CP violation in the Higgs-gauge sector. The phenomenological footprint of the associated anomalous couplings can be small, and designing measurement strategies with the highest sensitivity is therefore of the utmost importance in order to maximize the discovery potential of the Large Hadron Collider. There are, however, very few measurements of CP-sensitive observables in processes that probe the weak-boson self-interactions. In this article, we study the sensitivity to new sources of CP violation for a range of experimentally accessible electroweak processes, including $W\gamma$ production, WW production via photon fusion, electroweak Zjj production, electroweak $ZZjj$ production, and electroweak $W^{\pm}W^{\pm}jj$ production. We study simple angular observables as well CP-sensitive observables constructed using the outputs of machine-learning algorithms. We find that the machine-learning-constructed CP-sensitive observables improve the sensitivity to CP-violating effects by up to a factor of five, depending on the process. We also find that inclusive $W\gamma$ and electroweak Zjj production have the potential to set the best possible constraints on certain CP-odd operators in the Higgs-gauge sector of dimension-six effective field theories.

DOI: 10.1103/PhysRevD.107.016008

I. INTRODUCTION

Ten years after the Higgs boson discovery at CERN [1,2], the search for a more complete picture of particle physics than the Standard Model (SM) continues. With mounting pressure on traditionally motivated new-physics scenarios, measurements and searches increasingly aim to produce model-independent constraints, chiefly through the application of effective field theory methods [3]. Such approaches imply a plethora of *ad hoc* anomalous interactions between SM particles and suggest a wide range of possible physics analyses at the Large Hadron Collider (LHC), even when a weak doublet character of the Higgs field is assumed [4,5]. In contrast, a range of astrophysical and cosmological facts have been established that cannot be explained by the SM alone. These highlight particular subsectors of the effective field theory (EFT) deformations as particularly motivated beyond the SM (BSM) candidates for independent investigations. For instance, there is insufficient CP violation in the SM to explain the observed dominance of matter over antimatter in the Universe, which could indicate the need for additional CP-violating gauge-Higgs interactions.

The SMEFT extends the SM Lagrangian with CP-odd dimension-six operators, i.e.,

$$\mathcal{L} = \mathcal{L}_{\mathrm{SM}} + \sum_i \frac{c_i}{\Lambda^2}\tilde{\mathcal{O}}_i. \tag{1}$$

The Wilson coefficients, c_i/Λ^2, specify the strength of the anomalous interactions that are induced, and Λ is considered as the cutoff scale for the effective theory. Of particular interest are operators that affect the interactions between the Higgs boson and the electroweak bosons, or the self-interactions of the weak bosons, namely

$$\begin{aligned}
\tilde{\mathcal{O}}_{\tilde{W}} &= \varepsilon_{ijk}\tilde{W}^i_{\mu\nu}W^{j\nu\rho}W^{k\mu}_{\rho},\\
\tilde{\mathcal{O}}_{\Phi\tilde{B}} &= \Phi^{\dagger}\Phi B^{\mu\nu}\tilde{B}_{\mu\nu},\\
\tilde{\mathcal{O}}_{\Phi\tilde{W}} &= \Phi^{\dagger}\Phi W^{i\,\mu\nu}\tilde{W}^i_{\mu\nu},\\
\tilde{\mathcal{O}}_{\Phi\tilde{W}B} &= \Phi^{\dagger}\sigma^i\tilde{W}^{i\,\mu\nu}B_{\mu\nu}.
\end{aligned} \tag{2}$$

$W^i_{\mu\nu}$ and $B_{\mu\nu}$ are the $SU(2)_L \times U(1)_Y$ field strengths, the tilded quantities refer to the dual field strengths, σ^i are the

*christoph.englert@glasgow.ac.uk
†andrew.pilkington@manchester.ac.uk

Pauli matrices, and Φ denotes the Higgs doublet field. These interactions not only fully parametrize additional sources of weak CP-violating gauge-Higgs interactions, but they also form a closed set under the dimension-six renormalization group flow [6–8] so that their constraints form a theoretically consistent subset of CP violation for matching calculations (e.g., these interactions fully parametrize a broad class of lepton extensions of the SM [9,10], for a more general discussion see also [11]).

The beyond-the-SM matrix element for a given process following Eq. (1) is given by

$$|\mathcal{M}_{\mathrm{BSM}}|^2 = |\mathcal{M}_{\mathrm{SM}}|^2 + 2\mathrm{Re}\{\mathcal{M}_{\mathrm{SM}}\mathcal{M}_{\mathrm{d6}}^*\} + |\mathcal{M}_{\mathrm{d6}}|^2. \quad (3)$$

The dimension-six amplitude, $\mathcal{M}_{\mathrm{d6}}$, arises from the interactions induced by the operators of Eq. (2), whereas the SM amplitude, $\mathcal{M}_{\mathrm{SM}}$, arises from $\mathcal{L}_{\mathrm{SM}}$. The interference between the SM amplitude and the dimension-six amplitude induces asymmetries in appropriately constructed $(C)P$-odd observables.

In the Higgs sector, searches for new sources of CP-violation have received considerable attention by the LHC experiments in recent years, with particular emphasis on constructing CP-sensitive observables [12–19]. Efforts to maximize the sensitivity are necessary and underway, and observables constructed using matrix-element information are part of the existing analysis strategy [16–19]. Furthermore, machine-learning (ML) approaches have been proposed as an additional or alternative way to improve sensitivity to the asymmetries caused by new sources of CP violation [20–25]. Specifically, these ML approaches can be used to design highly sensitive physics analyses when the CP-violating effects are difficult to observe. The machine-learning methods are also relatively easy to implement when compared to matrix-element-based techniques.

In comparison to the Higgs sector, surprisingly little attention has been paid to constructing CP-sensitive observables in processes sensitive to weak-boson self-interactions. This is despite the fact that the CP-odd operators in Eq. (2) induce anomalous weak-boson self-interactions and can be probed using measurements of diboson production and weak-boson fusion/scattering. The ATLAS measurement of a CP-sensitive observable in electroweak Zjj production [26] provided world-leading linearized constraints on $c_{\tilde{W}}/\Lambda^2$ and limits on $c_{\Phi\tilde{W}B}/\Lambda^2$ that are competitive with those obtained from the Higgs sector. These constraints were derived using a simple angular observable, the rapidity-ordered azimuthal angle between the two jets (originally proposed in Ref. [27]), without attempting to use the more sophisticated techniques based on matrix-element information or machine-learning algorithms. Similarly, it was recently proposed that measurements of CP-sensitive observables in $W\gamma$ production would provide even better sensitivity to the $c_{\Phi\tilde{W}B}/\Lambda^2$ operator than was achieved in the electroweak Zjj analysis [28,29]. Again, that projection was based on simple angular observables and did not utilize matrix-element information or machine-learning algorithms.

In this paper, we use machine-learning algorithms to construct CP-sensitive observables for five processes that are sensitive to weak-boson self-interactions: electroweak Zjj production, inclusive $W\gamma$ production, electroweak $W^\pm W^\pm jj$ production, electroweak $ZZjj$ production, and photon-induced WW production ($\gamma\gamma \to WW$). We have two goals in this study. The primary goal is to motivate new analyses at the LHC experiments in order to address the paucity of measurements of CP-sensitive observables in the electroweak sector. A secondary goal is to test the applicability of the neural-net based method developed in Ref. [25] when constructing CP-sensitive observables in a wider range of processes.

The layout of the paper is as follows. In Sec. II, we give a brief introduction of our simulation framework, where we also provide an overview of the fiducial search regions used for this study. After a discussion of CP-sensitive observables in Sec. III, we outline the analysis selection and limit setting procedure in Sec. IV. Section V is devoted to the discussion of our results; we summarize and conclude in Sec. VI.

II. SIMULATION FRAMEWORK

Throughout, we use MadGraph5_aMC@NLO [30] which interfaced with PYTHIA 8 [31,32] to simulate events at leading-order precision in QCD. We employ the SMEFTsim [33,34] implementation to model the effective interactions of Eq. (2) via the UFO [35] interface. We limit our analysis to interference effects $\sim\mathrm{Re}\{\mathcal{M}_{\mathrm{SM}}\mathcal{M}_{\mathrm{d6}}^*\}$ of Eq. (3) and the simulated events are produced at $c/\Lambda^2 = 1/\mathrm{TeV}^2$. "Squared" CP-even dimension-6 effects $\sim|\mathcal{M}_{\mathrm{d6}}|^2$ will not affect the discrimination that we study below and would only change the normalization of the cross sections as part of the limit setting. Normalization modifications do also arise from the CP-even counter parts of Eq. (2) amongst other SMEFT interactions. Hence, limiting ourselves to interference effects provides not only a conservative estimate of the CP-sensitivity reach below, but also targets "genuine" CP violation through designing tell-tale phenomenological discriminators through (ML-generalized) asymmetries. By attributing CP violation to the hard scattering matrix element, we also implicitly assume SM-like decays, hadronization etc.

We use the NNPDF30NLO (NNPDF23LO) parton distribution functions [36] and the default set of parameters that define the PYTHIA 8 setup for parton showering, hadronization and underlying event activity. For weak-boson fusion and weak-boson scattering processes, it is known that the default parton shower scheme produces too much quark and gluon radiation [37,38]. For EW Zjj production, which eventually will be analyzed in a fiducial region that rejects events with additional jet activity (see

Sec. IV), we simulate the SM and interference contributions using the dipole-recoil scheme for the initial-state radiation. For electroweak (EW) $ZZjj$ and EW $W^{\pm}W^{\pm}jj$ production, we simulate the SM and interference contributions using the default shower scheme and rescale the sample weights by the ratio $\sigma^{\mathrm{SM}}_{\mathrm{dipole}}/\sigma^{\mathrm{SM}}_{\mathrm{default}}$, where σ^{SM} is the SM cross section in the fiducial region of the analysis and "dipole" or "default" label the shower scheme used to generate the sample. In this latter case, we have checked that the cross section ratio remains approximately flat across the kinematic variables that are of interest in the analysis.

III. *CP*-SENSITIVE OBSERVABLES

A. Simple angular observables

CP-sensitive observables can be easily constructed using the difference in azimuthal angle between two final particles, i.e.,

$$\Delta\phi_{ij} = \phi_i - \phi_j, \tag{4}$$

where i and j are ordered in rapidity such that $y_i > y_j$.

The signed azimuthal angle between the jets, $\Delta\phi_{jj}$, is clearly P odd, and has traditionally been used to search for CP violation in measurements sensitive to weak boson fusion [27]. We therefore utilize $\Delta\phi_{jj}$ for our analysis of electroweak Zjj production, electroweak $W^{\pm}W^{\pm}jj$ production, and electroweak $ZZjj$ production. For the inclusive $W\gamma$, $\gamma\gamma \to WW$ and electroweak $W^{\pm}W^{\pm}jj$ processes, the signed azimuthal angles between charged leptons and photons, $\Delta\phi_{\ell\gamma}$ and $\Delta\phi_{\ell\ell}$, can be constructed as *CP*-sensitive observables.

For the electroweak $ZZjj$ process, there are four charged leptons in the final state. *CP*-violating effects can be probed using the $\Phi_{4\ell}$ variable [39,40] defined by

$$\Phi_{4\ell} = \frac{\mathbf{q}_1 \cdot (\hat{\mathbf{n}}_1 \times \hat{\mathbf{n}}_2)}{|\mathbf{q}_1 \cdot (\hat{\mathbf{n}}_1 \times \hat{\mathbf{n}}_2)|} \times \cos^{-1}(\hat{\mathbf{n}}_1 \cdot \hat{\mathbf{n}}_2), \tag{5}$$

which measures the signed angle between the decay planes of the two Z bosons. Here, the normal vectors to the Z-boson decay planes are defined as

$$\hat{\mathbf{n}}_1 = \frac{\mathbf{q}_{11} \times \mathbf{q}_{12}}{|\mathbf{q}_{11} \times \mathbf{q}_{12}|} \quad \text{and} \quad \hat{\mathbf{n}}_2 = \frac{\mathbf{q}_{21} \times \mathbf{q}_{22}}{|\mathbf{q}_{21} \times \mathbf{q}_{22}|}, \tag{6}$$

where $\mathbf{q}_{\alpha\beta}$ represents the momentum of the lepton (or antilepton) β that originates from the decay $Z_\alpha \to \ell\bar{\ell}$. The $\mathbf{q}_\alpha = \mathbf{q}_{\alpha 1} + \mathbf{q}_{\alpha 2}$ is the corresponding momentum of the Z_α.

B. Observables constructed using neural networks

CP-sensitive observables can also be constructed using neural networks [25]. Specifically, for a given interference contribution, the event sample can be divided into positively weighted and negatively weighted events. The neural network can then be trained to separate the two classes in a binary classification. The SM prediction can be included in the training to simultaneously optimize the separation of the interference contributions from the SM contribution. This is referred to as a multiclass model. We mainly focus on the use of multiclass models in this article.

The *CP*-sensitive observables can be defined on an event-by-event basis using the trained models, i.e.,

$$O_{NN} = P_+ - P_-, \tag{7}$$

where P_+ and P_- are the probabilities that an event is a positively weighted or negatively weighted event, respectively. For a binary classification, $P_+ + P_- = 1$. For a multiclass model, $P_+ + P_- + P_{\mathrm{SM}} = 1$, where P_{SM} is the probability that an event is a SM event.

We use TensorFlow 2.3.0 [41] to train the neural networks. The input variables are the transverse momentum (p_{T}), pseudorapidity (η), and azimuthal angle ϕ of each visible particle that defines the final state (i.e., leptons, photons, and jets). Lepton flavor and charge are also included, though found to add little sensitivity. In addition, the magnitude ($E^{\mathrm{miss}}_{\mathrm{T}}$) and angle ($\phi_{\mathrm{miss}}$) of the missing transverse momentum are included for $W\gamma$ production. The choice of hyperparameters is optimized for each network and obtained using the KERAS suite [42,43]. The optimization included the number of layers, the number of nodes, the learning rate and the batch size. A data augmentation procedure was used to prevent the networks learning features that arise from statistical fluctuations. In this procedure, each event is used twice in the training, once with the default input variables and once with a *CP* operator applied to each of the input variables. The event weight is multiplied by -1 for the *CP*-flipped events in the interference sample.

IV. ANALYSIS METHODOLOGY

For each process, we apply the selection cuts used in a recent ATLAS or CMS analysis and, where possible, validate our event generation by comparing the SM fiducial cross section that we obtain from our simulated samples to the theoretical values quoted in the relevant publication. Table I presents our fiducial cross sections, which are in good agreement with those reported in the literature after considering differences such as leading-order predictions versus next-to-leading order predictions (in particular in $W\gamma$ production these can be sizeable [44,45]).[1]

To determine the sensitivity, we construct confidence intervals from each of the *CP*-odd observables of Sec. III by means of a binned likelihood function

[1]For EW $ZZjj$ production, we only generate the $ZZ \to 2e2\mu$ final state and our cross section is therefore a factor of 2 smaller than the theoretical prediction used in Ref. [46].

TABLE I. SM fiducial cross sections and event yield normalizations for each of the processes studied in this paper. The fiducial cross sections are calculated within the fiducial region of an ATLAS or CMS experimental analysis and found to be in good agreement with the theoretical predictions reported in those papers. The uncertainties quoted on the fiducial cross sections are statistical and do not contain any systematic uncertainties in the theoretical calculations. The normalization of the samples is needed for the limit setting and the yields quoted apply to the signal processes. The treatment of backgrounds is discussed in the text.

Process	Fiducial region	SM cross section	SM yield normalization (limit setting only)
EW Zjj ($Z \to \ell\ell$)	Ref. [26] (signal region)	$33.9 \pm 0.1(\text{stat})$ fb	3712 [26]
inclusive $W\gamma$ ($W \to \ell\nu$)	Ref. [47] (Sec. VI)	$294 \pm 1(\text{stat})$ fb	102191 [47]
EW $ZZjj$ ($ZZ \to 2e2\mu$))	Ref. [46]	$0.09 \pm 0.01(\text{stat})$ fb	22.4 [46]
EW $W^{\pm}W^{\pm}jj$ ($W \to \ell\nu$)	Ref. [48]	$2.19 \pm 0.01(\text{stat})$ fb	60 [48]
elastic $\gamma\gamma \to WW$ ($W \to \ell\nu$)	Ref. [49] (signal region)	$0.67 \pm 0.01(\text{stat})$ fb	174 [49]

$$\mathcal{L}(\{c_j\}/\Lambda^2) = \prod_k \exp\{-\lambda_k\}\frac{\lambda_k^{n_k}}{n_k!}. \tag{8}$$

Here, k labels the bins with n_k denoting the expected number of events in bin k assuming the SM-only hypothesis. λ_k is the predicted number of events given the SMEFT hypothesis, which is derived from a particular parameter choice in Wilson coefficient space $\{c_j\}/\Lambda^2$. The likelihood of Eq. (8) is converted to a confidence level via a profile-likelihood test statistic [50]. Through Wilks's theorem [51], we can assume this statistic to be distributed according to a χ^2 distribution with one degree of freedom, from which the 95% confidence level can be obtained. The likelihood function does not include terms that account for systematic uncertainties. This is justified because the constraints are driven by asymmetries in the CP-odd observables, whereas the impact of systematic uncertainties on those distributions would be symmetric. The potential impact of systematic uncertainties is investigated further in Sec. V D.

The λ_k and n_k in Eq. (8) are directly derived from the simulated samples, after applying normalization factors to convert the predicted cross sections into event yields. The normalization factor is defined for each process such that the SM prediction reproduces the number of SM events that were predicted in the relevant fiducial regions of the ATLAS or CMS analysis (see Table I). This normalization factor is applied to both the SM signal prediction and the interference contribution. For the EW Zjj process, the effect of non-EW Zjj backgrounds is included in the calculation of λ_k and n_k by generating a QCD Zjj sample at $\mathcal{O}(\alpha_s^2\alpha)$ and normalizing that sample to the observed signal-subtracted number of Zjj events observed in Ref. [26]. For all other processes, the effects of backgrounds are included in the calculation of λ_k and n_k by scaling the SM signal sample to reproduce the number of background events reported in the relevant experimental analysis. This latter approach assumes the kinematic properties of the SM signal and the background are sufficiently similar.

The choice of binning can impact the final confidence level and it is therefore convenient to optimize the binning is such a way that the sensitivity is maximized. Typically about 20 bins are chosen per distribution, with bins subsequently merged to ensure that there is at least one SM event per bin. Postfit, we check that the theoretical prediction remains positive at the values of the Wilson coefficient that correspond to the 95% C.L., and merge bins if this is not the case.

V. RESULTS

A. EW *Zjj* and inclusive *Wγ* production

The differential cross section for EW Zjj production as a function of $\Delta\phi_{jj}$ is shown in Fig. 1. Figure 2 shows the differential cross section for inclusive $W\gamma$ production as a function of $\Delta\phi_{\ell\gamma}$. In both cases, the SM prediction is shown in addition to the interference contributions induced by the $\mathcal{O}_{\Phi\tilde{W}B}$ and $\mathcal{O}_{\tilde{W}}$ operators, with Wilson coefficients set to $c/\Lambda^2 = 1$ TeV^{-2}. As expected, the CP-even SM prediction is symmetric about $\Delta\phi_{jj}$, $\Delta\phi_{\ell\gamma} = 0$, whereas the CP-odd interference contributions are all asymmetric with an integral of zero. For these simple angular variables, EW Zjj production is most sensitive to the $\mathcal{O}_{\tilde{W}}$ operator,

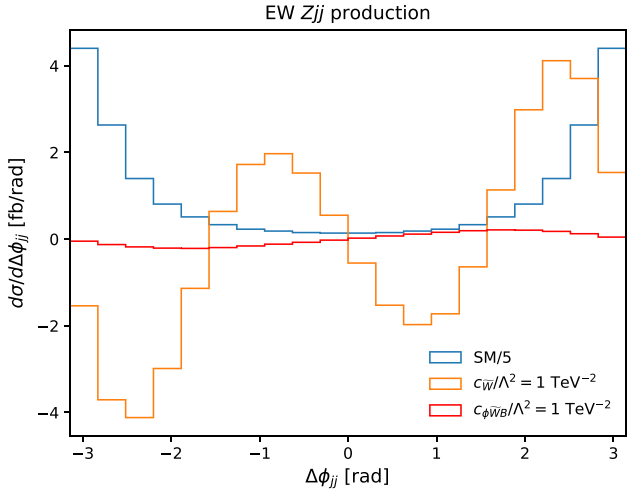

FIG. 1. Differential cross sections for the SM and the interference contributions to EW Zjj production as a function of the CP-odd observable $\Delta\phi_{jj}$. The interference contributions are shown for the $\mathcal{O}_{\tilde{W}}$ and $\mathcal{O}_{\Phi\tilde{W}B}$ operators.

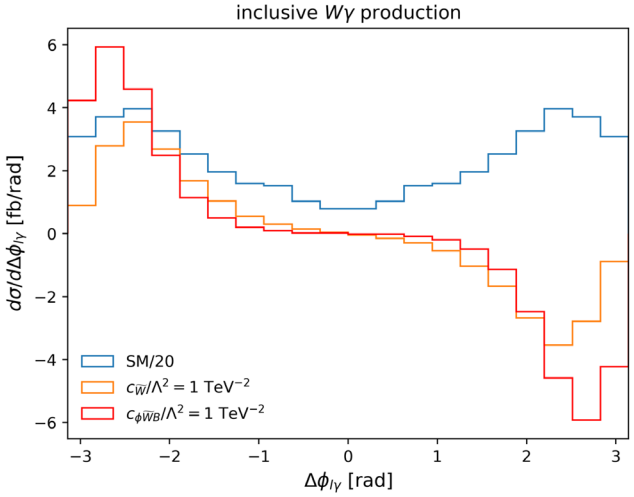

FIG. 2. Differential cross sections for the SM and the interference contributions to inclusive $W\gamma$ production as a function of the CP-odd observable $\Delta\phi_{\ell\gamma}$. The interference contributions are shown for the $\mathcal{O}_{\tilde{W}}$ and $\mathcal{O}_{\Phi\tilde{W}B}$ operators.

whereas inclusive $W\gamma$ production is roughly equally sensitive to both operators.

The differential cross section for EW Zjj production as a function of the CP-odd observable produced by a multiclass neural network is shown in Fig. 3. The corresponding distribution for inclusive $W\gamma$ production is shown in Fig. 4. For each operator and process, a neural network is trained to distinguish between the positively weighted interference contribution, the negatively weighted interference contribution, and the contribution from the SM. This leads to a different SM distribution depending on the operator being

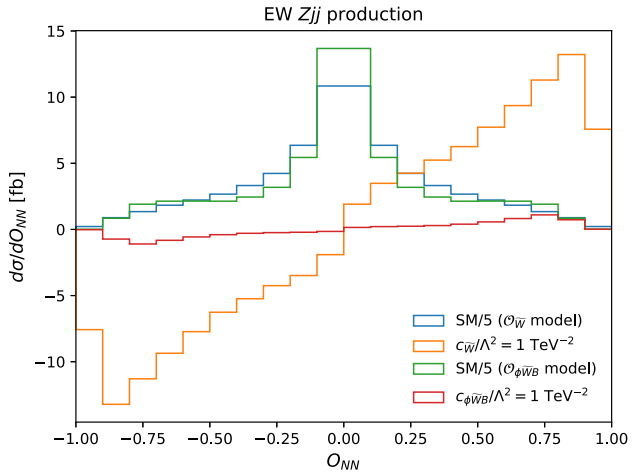

FIG. 3. Differential cross sections for the SM and the interference contributions to EW Zjj production as a function of the CP-odd observable O_{NN} (multiclass model). The interference contributions are shown for the $\mathcal{O}_{\tilde{W}}$ and $\mathcal{O}_{\Phi\tilde{W}B}$ operators. The neural network was trained separately for each interference contribution.

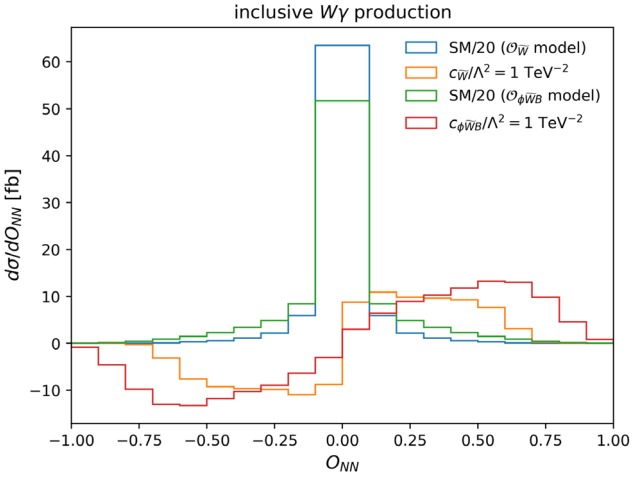

FIG. 4. Differential cross sections for the SM and the interference contributions to inclusive $W\gamma$ production as a function of the CP-odd observable O_{NN} (multiclass model). The interference contributions are shown for the $\mathcal{O}_{\tilde{W}}$ and $\mathcal{O}_{\Phi\tilde{W}B}$ operators. The neural network was trained separately for each interference contribution.

tested. The interference contributions are presented for $c_{\Phi\tilde{W}B}/\Lambda^2 = 1\ \text{TeV}^{-2}$ and $c_{\tilde{W}}/\Lambda^2 = 1\ \text{TeV}^{-2}$.

For both processes, the network is effective at separating the positively weighted and negatively weighted interference contributions, with the positively weighted events peaking close to $O_{NN} > 0.5$ and the negatively weighted events at $O_{NN} < -0.5$. The SM contribution is symmetric and peaked at output values very close to zero. In the case of inclusive $W\gamma$ production, it is clear that the network has improved the sensitivity over the use of $\Delta\phi_{\ell\gamma}$ alone, because the interference contributions are much larger relative to the SM prediction.

To quantify the sensitivity of the different observables, we use the profile-likelihood test outlined in Sec. IV. The constraints obtained for each Wilson coefficient are shown in Table II. For EW Zjj production, the expected 95% confidence intervals obtained from fits to the $\Delta\phi_{jj}$ distribution are similar to those reported by the ATLAS Collaboration [26], with up to 30% improvement (for $c_{\tilde{W}}/\Lambda^2$) that is due to (i) using more finely binned distributions[2] and (ii) the small effect of missing systematic uncertainties. For inclusive $W\gamma$ production, the 95% confidence intervals obtained from fits to the $\Delta\phi_{l\gamma}$ distribution are similar to those reported in Ref. [11]. The good agreement between our results and those previously reported indicates that our simulation (and subsequent event normalization) can be used to assess the sensitivity to the different CP-sensitive observables.

[2]This is a consequence of the ATLAS measurement being unfolded and requiring more events per bin of the distribution.

TABLE II. Expected 95% confidence interval for the Wilson coefficients affecting triple gauge couplings given an integrated luminosity of 139 fb^{-1} for EW Zjj and inclusive $W\gamma$ production. Results are presented for a one-dimensional fit to the relevant signed-azimuthal angle distribution for each process, as well as fits to the O_{NN} variable constructed from the neural-net outputs of the multiclass models. Each O_{NN} variable is constructed using the interference predicted by the specific operator being tested.

Process	CP-odd observable	$c_{\Phi\tilde{W}B}/\Lambda^2$ [TeV^{-2}]	$c_{\tilde{W}}/\Lambda^2$ [TeV^{-2}]
EW Zjj	$\Delta\phi_{jj}$	$[-1.05, 1.05]$	$[-0.081, 0.081]$
	O_{NN} (multiclass)	$[-0.83, 0.83]$	$[-0.047, 0.047]$
	$\Delta\phi_{jj}$ vs $\Delta\phi_{\ell\ell}$	$[-0.99, 0.99]$	$[-0.074, 0.074]$
	$\Delta\phi_{jj}$ vs $p_{\mathrm{T},\ell\ell}$	$[-1.04, 1.04]$	$[-0.066, 0.066]$
inclusive $W\gamma$	$\Delta\phi_{l\gamma}$	$[-0.165, 0.165]$	$[-0.255, 0.255]$
	O_{NN} (multiclass)	$[-0.049, 0.049]$	$[-0.056, 0.056]$
	$\Delta\phi_{l\gamma}$ vs $\lvert\phi_l - \phi_{\mathrm{miss}}\rvert$	$[-0.154, 0.154]$	$[-0.219, 0.219]$
	$\Delta\phi_{l\gamma}$ vs $E_{\mathrm{T}}^{\mathrm{miss}}$	$[-0.163, 0.163]$	$[-0.206, 0.206]$

The CP-sensitive observables constructed from the output of a multiclass neural network provide much better sensitivity than the simple angular observables alone, with 95% confidence intervals reduced by a factor of up to 2 for EW Zjj production and by a factor of 3–5 for inclusive $W\gamma$ production, depending on the specific dimension-six operator. This improvement is similar to that seen in studies of Higgs boson final states in Ref. [25]. Using the O_{NN} observable, the EW Zjj and inclusive $W\gamma$ processes provide similar sensitivity to CP-violating effects induced by the $\mathcal{O}_{\tilde{W}}$ operator. The best current experimental constraints on this operator using linearized EFT contributions are those reported by ATLAS using the $\Delta\phi_{jj}$ distribution in EW Zjj production, i.e., $-0.11 < c_{\tilde{W}}(\mathrm{TeV}/\Lambda)^2 < 0.14$, a factor of 2 less sensitive. Thus the use of neural networks to construct the CP-sensitive observable and expanding the CP-sensitive measurements to the inclusive $W\gamma$ final state will dramatically improve the sensitivity in the future. For the $\mathcal{O}_{\Phi\tilde{W}B}$ operator, the constraints obtained from inclusive $W\gamma$ production will be a factor of 17 more precise than can be obtained from measurement of EW Zjj production. This is an important result, because the ATLAS collaboration measured $0.23 < c_{\Phi\tilde{W}B}(\mathrm{TeV}/\Lambda)^2 < 2.34$ using the $\Delta\phi_{jj}$ distribution in EW Zjj production, with the SM prediction being outside of the 95% confidence interval.[3] The measurements of CP-sensitive observables such as O_{NN} for inclusive $W\gamma$ production are therefore critical in searches for CP-violating effects in the Higgs-gauge sector.

The improved constraints obtained with the CP-sensitive observables constructed using neural networks can be investigated using feature importance techniques. In this approach, the importance of each input variable to the trained network is determined, by evaluating the decrease in accuracy that occurs when the values of the input variable are randomly interchanged in the dataset. An example is shown in Fig. 5 for the multiclass network trained on EW Zjj events, with the interference contribution produced by the $\mathcal{O}_{\Phi\tilde{W}B}$ operator. As expected, the most important variables are the azimuthal angles and rapidities of the two jets, which are needed for the network to learn the $\Delta\phi_{jj}$ observable. However, the azimuthal angles and rapidities of the two leptons are also important, which we trace back to an underlying asymmetry in the $\Delta\phi_{\ell\ell}$ observable, and the network is also exploiting to distinguish between positive and negative interference effects. Finally, the transverse momentum of the two leptons is also important in the multiclass network. However, in our cross check using a binary network, the lepton transverse momentum is not considered to be important. This means that the multiclass network is using the lepton transverse momentum to distinguish between the SM prediction and the interference contributions.

We can use the information from the feature importance tests to construct double-differential distributions that are

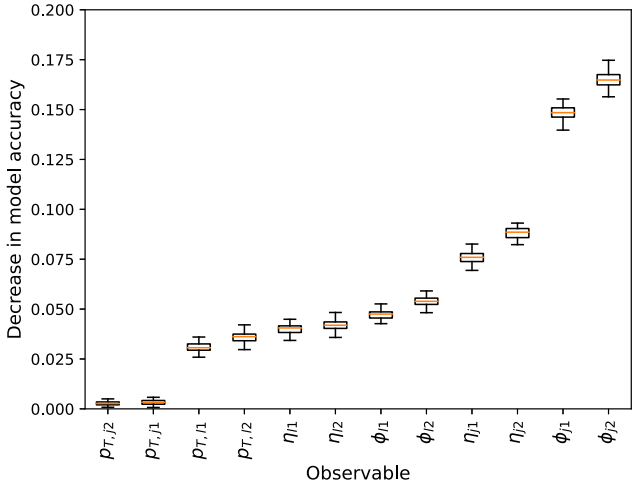

FIG. 5. Feature importance for the multiclass network trained on EW Zjj events, with the interference contribution produced by the $\mathcal{O}_{\Phi\tilde{W}B}$ operator.

[3]This slight asymmetry is not considered to be significant when considering the global p value [26].

more sensitive than the simple angular variables alone. The 95% confidence intervals obtained from (i) a two-dimensional fit to $\Delta\phi_{jj}$ and $\Delta\phi_{\ell\ell}$, as well as (ii) a two-dimensional fit to $\Delta\phi_{jj}$ and $p_{\mathrm{T},\ell\ell}$, are also shown in Table II. For both operators, the constraints are improved using a two-dimensional fit when compared to the use of the simple angular variable alone, but remain inferior to those obtained using a fit to the O_{NN} observable.

For inclusive $W\gamma$ production, the feature importance tests highlight the importance of the rapidities and azimuthal angles of the lepton and the photon, as expected. However, the azimuthal angle of the missing transverse momentum vector is also found to be important, along with the magnitude of the missing transverse momentum and the transverse momenta of the lepton and photon. The 95% confidence intervals were determined for a variety of two-dimensional fits to double-differential distributions; the constraints obtained using a two-dimensional fit to $\Delta\phi_{\ell\gamma}$ and $E_{\mathrm{T}}^{\mathrm{miss}}$ is shown in Table II, those obtained from a two-dimensional fit to $\Delta\phi_{\ell\gamma}$ and the difference between the azimuthal angles of the lepton and the missing transverse momentum vector. Again, the constraints on the Wilson coefficients are improved with respect to the simple angular variable alone, but do not recover the full sensitivity of the *CP*-sensitive observable constructed from the output of the multiclass network.

In summary, these two examples demonstrate that *CP*-sensitive observables constructed using machine-learning techniques can dramatically improve the LHC experiments' sensitivity to *CP*-violating effects in dimension-six effective field theories.

B. EW $W^{\pm}W^{\pm}jj$, EW $ZZjj$, and $\gamma\gamma \to WW$ production

In this section, we turn our attention to the processes sensitive to the interaction between four electroweak bosons, namely electroweak $W^{\pm}W^{\pm}jj$ production, electroweak $ZZjj$ production, and $\gamma\gamma WW$ production. These scattering processes have a significantly reduced SM cross section compared to inclusive $W\gamma$ and EW Zjj production as shown in Table I, and we can therefore expect these processes to play a less relevant role in constraining the dimension-six operators investigated in this article. Nevertheless, the applicability of machine-learning methods in constructing *CP*-sensitive observables can still be investigated for each process, which could prove important in the longer term if the LHC experiments start to search for *CP*-violating effects predicted by dimension-eight effective field theories where multi-gauge boson interactions provide complementary tests to, e.g., ZZZ-related interactions (see [52–56]).

The 95% confidence intervals obtained for the Wilson coefficients are presented in Table III, where for each process and operator the constraints obtained using simple angular observables are compared to the constraints obtained using the O_{NN} observable constructed from the output of a multiclass network. These results are obtained by following all of the steps outlined in the previous sections regarding the ML training and limit setting. In general, many of the constraints in Table III indicate general insensitivity to *CP* violation as predicted by dimension-six effective field theory and are much less sensitive than those obtained for inclusive $W\gamma$ production and EW Zjj production in Sec. V A. However, it is also clear that employing the ML-driven observables leads to significant improvement in sensitivity when compared to the simple angular observables alone.

In the case of EW $W^{\pm}W^{\pm}jj$ production, the O_{NN} observable is sufficiently sensitive to the *CP*-violating effects predicted $\mathcal{O}_{\tilde{W}}$ operator and experimental measurements of O_{NN} for this process would provide useful additional information in a global fit. Unsurprisingly, the sensitivity is mainly driven by the $\Delta\phi_{jj}$ distribution, the differential cross section for which is shown in Fig. 6.

TABLE III. Expected 95% confidence interval for representative Wilson coefficients given an integrated luminosity of 139 fb^{-1}. Limits are not competitive in comparison to the trilinear coupling sensitivity of Zjj and $W\gamma$ production. To this end we focus on a motivated subset of operators for $ZZjj$ and $W^{\pm}W^{\pm}jj$ production: Z-photon mixing highlights $ZZjj$ production as a probe for B-like operators as compared to $WWjj$ production. Results are again presented for simple angular observables and for the O_{NN} variable constructed from the outputs of the multiclass networks. Each O_{NN} variable is constructed using the interference predicted by the specific operator being tested.

Process	*CP*-odd observable	$c_{\Phi\tilde{W}B}/\Lambda^2$ [TeV^{-2}]	$c_{\Phi\tilde{B}}/\Lambda^2$ [TeV^{-2}]	$c_{\Phi\tilde{W}}/\Lambda^2$ [TeV^{-2}]	$c_{\tilde{W}}/\Lambda^2$ [TeV^{-2}]
EW $ZZjj$	$\Delta\phi_{jj}$	$[-3.7, 3.7]$	$[-43, 43]$	⋯	⋯
	$\Phi_{4\ell}$	$[-51, 51]$	$[-64, 64]$	⋯	⋯
	O_{NN} (multiclass)	$[-3.0, 3.0]$	$[-12, 12]$	⋯	⋯
EW $W^{\pm}W^{\pm}jj$	$\Delta\phi_{jj}$	⋯	⋯	$[-35, 34]$	$[-1.83, 1.83]$
	$\Delta\phi_{\ell\ell}$	⋯	⋯	$[-105, 105]$	$[-14, 14]$
	O_{NN} (multiclass)	⋯	⋯	$[-17, 17]$	$[-0.76, 0.76]$
$\gamma\gamma \to WW$	$\Delta\phi_{\ell\ell}$	$[-32, 32]$	$[-14, 14]$	$[-48, 48]$	$[-19, 19]$
	O_{NN} (multiclass)	$[-11, 11]$	$[-13, 13]$	$[-43, 43]$	$[-11, 11]$

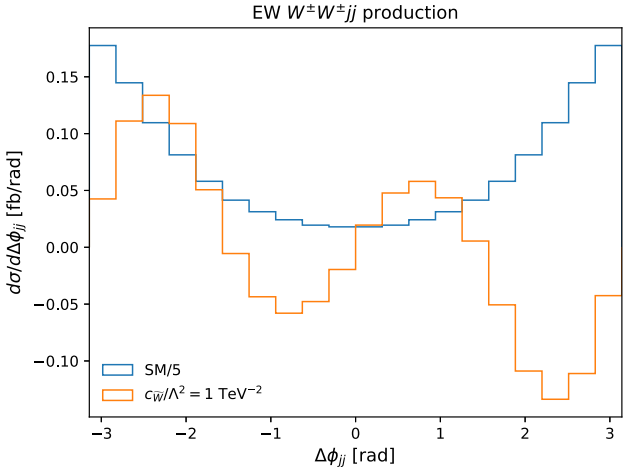

FIG. 6. Differential cross sections for the SM and the interference contributions to EW $W^\pm W^\pm jj$ production as a function of the CP-odd observable $\Delta\phi_{jj}$. The interference contribution is shown for the $\mathcal{O}_{\tilde{W}}$ operator.

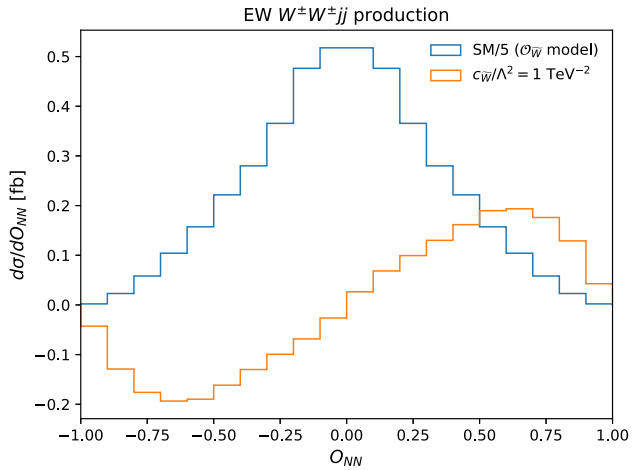

FIG. 7. Differential cross sections for the SM and the interference contributions to EW $W^\pm W^\pm jj$ production as a function of the ML-constructed CP-odd observable O_{NN}. The interference contribution is shown for the $\mathcal{O}_{\tilde{W}}$ operator.

However, the fits to the ML-constructed observable improves the constraints by a factor of about 2.5. Figure 7 shows the differential cross section as a function of O_{NN}, where the asymmetry is clearly enhanced with respect to the SM prediction when compared to the $\Delta\phi_{jj}$ distribution.

C. Extrapolation to high luminosity LHC

The constraints obtained on the Wilson coefficients will improve further in the high-luminosity (HL) phase of the LHC, where the expected integrated luminosity will reach 3 ab^{-1} per experiment. In Table IV we present the constraints obtained using the O_{NN} variable constructed from a multiclass model. For these results, the binning was reoptimized, following the procedure outlined in Sec. IV and allowing a larger number of bins to reflect the increased event yields expected at the HL-LHC. In general we find that allowing finer binning does not lead to an improvement in the 95% confidence intervals obtained for each Wilson coefficient. The constraints therefore improve by approximately the ratio $(L_{\text{HL-LHC}}/L_{\text{LHC}})^{1/2}$, where L is the integrated luminosity of the dataset (at HL-LHC or LHC as appropriate). This scaling also shows that the sensitivity is dominated by an inclusive selection channeled into the neural-net-based observable, without targeting exclusive phase space regions that become populated at the HL-LHC. Systematic uncertainties of the current LHC runs (see below) will therefore qualitatively carry over to the HL-LHC.

D. Impact of systematic uncertainties

The constraints on the Wilson coefficients presented in the previous sections have been estimated without considering the effect of systematic uncertainties. Although such uncertainties can be large, they will be symmetric as function of a given CP-sensitive observable. In the profile likelihood, therefore, any pull on the associated nuisance parameter to account for asymmetric deviations from the SM prediction would improve the agreement between data and theory in only half of the bins in the distribution, with poorer agreement obtained in the other half of the bins. This should reduce the impact of systematic uncertainties on the 95% confidence intervals obtained for CP-odd operators.

To demonstrate this effect, we introduce systematic uncertainties in the likelihood function for EW Zjj

TABLE IV. Expected 95% confidence interval for representative Wilson coefficients given an integrated luminosity of 3 ab^{-1} (HL-LHC). Results are presented for the O_{NN} variable. The O_{NN} variable is constructed from a multiclass network that is trained on the interference predicted by the specific operator being tested. Again, we focus on a motivated subset of operators for each production channel.

Process	$c_{\Phi\tilde{W}B}/\Lambda^2$ [TeV^{-2}]	$c_{\Phi\tilde{B}}/\Lambda^2$ [TeV^{-2}]	$c_{\Phi\tilde{W}}/\Lambda^2$ [TeV^{-2}]	$c_{\tilde{W}}/\Lambda^2$ [TeV^{-2}]
EW Zjj	$[-0.18, 0.18]$	⋯	⋯	$[-0.010, 0.010]$
inclusive $W\gamma$	$[-0.010, 0.010]$	⋯	⋯	$[-0.012, 0.012]$
EW $ZZjj$	$[-0.66, 0.66]$	$[-2.4, 2.4]$	⋯	⋯
EW $W^\pm W^\pm jj$	⋯	⋯	$[-3.9, 3.9]$	$[-0.19, 0.19]$
$\gamma\gamma \to WW$	$[-2.5, 2.5]$	$[-2.7, 2.7]$	$[-9.6, 9.6]$	$[-2.5, 2.5]$

production and inclusive $W\gamma$ production. For each of these processes, the likelihood function is modified to include a single Gaussian-constrained nuisance parameter, which is intended to account for the systematic uncertainties in the measurements and the theoretical uncertainties in the SM predictions. The dominant uncertainty for EW Zjj production arises from the theoretical modeling of the non-EW Zjj process, with sizeable contributions also from experimental (jet-energy-scale) uncertainties [57]. The total uncertainty is about 15% uncertainty at low-$|\Delta\phi_{jj}|$ and 25% at high-$|\Delta\phi_{jj}|$. A weak dependence is observed as a function of the Z-boson transverse momentum. For inclusive $W\gamma$ production, the combined experimental and theoretical uncertainty rises from 7% at low photon transverse momentum to about 25% at high transverse momentum [58]. However, the uncertainty is relatively flat as a function of angular observables.

The impact of the systematic uncertainties is first tested for EW Zjj production, with the Wilson coefficients constrained using the $|\Delta\phi_{jj}|$ distribution; we find that the 95% confidence intervals are increased by 1–2% with respect to those presented in Table II. This is similar to, but slightly smaller than, the effect reported by the ATLAS Collaboration, in which the systematic uncertainties increase the confidence intervals by about 4% (see the auxiliary material of Ref. [26]). It is likely that the smaller impact in our analysis is due to using a simplified model for systematic uncertainties, i.e., that the likelihood is too constraining on the single nuisance parameter. Dropping the Gaussian constraint on the nuisance parameter leads to a slightly larger impact of systematic uncertainties, with the 95% confidence intervals increased by 2–3% with respect to Table II.

The dependence of the systematic uncertainties as a function of O_{NN}, for both inclusive EW Zjj production and $W\gamma$ production, is not known and so both uniform and linear dependences are tested in the likelihoods. Again, the impact is small, with a 1% increase in the confidence intervals if the nuisance parameter has a Gaussian penalty term, and a 2–3% impact if it does not. From these studies, we conclude that systematic uncertainties will be modest in any future analysis at the LHC.

VI. CONCLUSIONS

The observed matter-antimatter asymmetry in the Universe requires new physics BSM and signposts specific areas for phenomenological scrutiny. Specifically, new sources of *CP* violation are required. Searches for *CP* violation at the LHC experiments increasingly aim to produce model-independent constraints through the application of effective field theories. Of particular interest is the possibility of *CP*-violating effects in the Higgs-gauge sector. Although the Higgs sector has received considerable attention along these lines recently, the search for *CP* violation using processes sensitive to the weak-boson self-interactions is much less explored. These processes however can provide similar sensitivity as the measurements in the Higgs sector, given the gauge structure of the relevant operators in the SMEFT. With this in mind, we have investigated a range of purely electroweak processes in this article, which are sensitive to the underlying nature of the weak-boson self-interactions.

Deviations from the SM are likely to be small, however, showing up predominantly as asymmetries in *CP*-sensitive observables. Enhancing the new physics reach of the LHC is therefore directly related to formulation of most sensitive BSM discriminators. "Traditional" angular observables, albeit theoretically motivated, might not provide the most sensitive approaches to uncover the anomalous interactions. Many (even termed "optimal") observables have been proposed, typically motivated by considering the angular decompositions of scattering processes. Their choice, however, is not unique. The appropriate choice of observables or observable combinations therefore becomes a question of optimization that feeds into an enhanced discovery potential at the LHC. This is the natural realm of ML, which will perform exactly the task of constructing a tailored *CP*-sensitive asymmetry optimized to new physics deformations that are parametrized consistently in the SMEFT.

We have employed the machine-learning techniques proposed in Ref. [25] to simultaneously construct the *CP*-sensitive observables and optimize the analysis sensitivity for each of the electroweak processes under investigation. We show that the ML-constructed *CP*-sensitive observables can lead to large sensitivity enhancements in searches for *CP* violation at the LHC. The ML algorithm (neural network) achieves this improvement using a multiclass model, which discriminates between the positive- and negative-interference contributions that describe the *CP*-violating effects, as well as between the interference contributions and the SM prediction.

We show that future measurements of ML-based *CP*-sensitive observables for inclusive $W\gamma$ production and EW Zjj production should each improve the sensitivity to *CP*-violating effects predicted by the $\mathcal{O}_{\tilde{W}}$ operator in the effective field theory by a factor of 2 compared to the current best constraints. We also show that the measurement of ML-based *CP*-sensitive observables for inclusive $W\gamma$ process can provide a factor of five improvement in sensitivity to the $\mathcal{O}_{\Phi\tilde{W}B}$ operator over the use of simple angular observables alone. This particular operator in the effective field theory is difficult to constrain; the measurement and technique outlined in this paper is likely to produce the best possible sensitivity.

Although the large improvements in sensitivity are a result of proof-of-principle analyses, they highlight the huge potential that ML-constructed *CP*-sensitive observables can unleash at the LHC, not only presently with the run-II and run-III datasets, but also during the high-luminosity phase in the future.

ACKNOWLEDGMENTS

C. E. is supported by the STFC under Grant No. ST/T000945/1, by the Leverhulme Trust under Grant No. RPG-2021-031, and the IPPP Associateship Scheme. A. D. P. is supported by the Royal Society and STFC under Grants No. UF160396, No. ST/S000925/1, and No. ST/W000601/1. R. H. and A. D. P. are supported by the Leverhulme Trust under Grant No. RPG-2020-004.

[1] G. Aad *et al.* (ATLAS Collaboration), Observation of a new particle in the search for the Standard Model Higgs boson with the ATLAS detector at the LHC, Phys. Lett. B **716**, 1 (2012).

[2] S. Chatrchyan *et al.* (CMS Collaboration), Observation of a New Boson at a Mass of 125 GeV with the CMS Experiment at the LHC, Phys. Lett. B **716**, 30 (2012).

[3] S. Weinberg, Phenomenological Lagrangians, Physica (Amsterdam) **96A**, 327 (1979).

[4] B. Grzadkowski, M. Iskrzynski, M. Misiak, and J. Rosiek, Dimension-six terms in the standard model Lagrangian, J. High Energy Phys. 10 (2010) 085.

[5] M. Baak, J. Cúth, J. Haller, A. Hoecker, R. Kogler, K. Mönig, M. Schott, and J. Stelzer (Gfitter Group Collaboration), The global electroweak fit at NNLO and prospects for the LHC and ILC, Eur. Phys. J. C **74**, 3046 (2014).

[6] R. Alonso, E. E. Jenkins, A. V. Manohar, and M. Trott, Renormalization group evolution of the standard model dimension six operators III: Gauge coupling dependence and phenomenology, J. High Energy Phys. 04 (2014) 159.

[7] C. Grojean, E. E. Jenkins, A. V. Manohar, and M. Trott, Renormalization group scaling of Higgs operators and $\Gamma(h \to \gamma\gamma)$, J. High Energy Phys. 04 (2013) 016.

[8] C. Englert and M. Spannowsky, Effective theories and measurements at colliders, Phys. Lett. B **740**, 8 (2015).

[9] S. D. Bakshi, J. Chakrabortty, C. Englert, M. Spannowsky, and P. Stylianou, Landscaping *CP*-violating BSM scenarios, Nucl. Phys. **B975**, 115676 (2022).

[10] W. Naskar, S. Prakash, and S. U. Rahaman, EFT Diagrammatica II: Tracing the UV origin of bosonic D6 CPV and D8 SMEFT operators, J. High Energy Phys. 08 (2022) 190.

[11] C. Degrande and J. Touchèque, A reduced basis for *CP* violation in SMEFT at colliders and its application to Diboson production, J. High Energy Phys. 04 (2022) 032.

[12] M. Aaboud *et al.* (ATLAS Collaboration), Measurements of Higgs boson properties in the diphoton decay channel with 36 fb^{-1} of pp collision data at $\sqrt{s} = 13$ TeV with the ATLAS detector, Phys. Rev. D **98**, 052005 (2018).

[13] G. Aad *et al.* (ATLAS Collaboration), Measurements of the Higgs boson inclusive and differential fiducial cross sections in the 4ℓ decay channel at $\sqrt{s} = 13$ TeV, Eur. Phys. J. C **80**, 942 (2020).

[14] G. Aad *et al.* (ATLAS Collaboration), Constraints on Higgs boson properties using $WW^*(\to e\nu\mu\nu)jj$ production in 36.1 fb^{-1} of $\sqrt{s} = 13$ TeV pp collisions with the ATLAS detector, Eur. Phys. J. C **82**, 622 (2022).

[15] A. Tumasyan *et al.* (CMS Collaboration), Analysis of the *CP* structure of the Yukawa coupling between the Higgs boson and τ leptons in proton-proton collisions at $\sqrt{s} = 13$ TeV, J. High Energy Phys. 06 (2022) 012.

[16] G. Aad *et al.* (ATLAS Collaboration), Test of *CP* invariance in vector-boson fusion production of the Higgs boson using the optimal observable method in the ditau decay channel with the ATLAS detector, Eur. Phys. J. C **76**, 658 (2016).

[17] A. M. Sirunyan *et al.* (CMS Collaboration), Constraints on anomalous HVV couplings from the production of Higgs bosons decaying to τ lepton pairs, Phys. Rev. D **100**, 112002 (2019).

[18] G. Aad *et al.* (ATLAS Collaboration), Test of *CP* invariance in vector-boson fusion production of the Higgs boson in the $H \to \tau\tau$ channel in proton-proton collisions at $\sqrt{s} =$ 13 TeV with the ATLAS detector, Phys. Lett. B **805**, 135426 (2020).

[19] A. M. Sirunyan *et al.* (CMS Collaboration), Constraints on anomalous Higgs boson couplings to vector bosons and fermions in its production and decay using the four-lepton final state, Phys. Rev. D **104**, 052004 (2021).

[20] J. Brehmer, F. Kling, T. Plehn, and T. M. P. Tait, Better Higgs-CP tests through information geometry, Phys. Rev. D **97**, 095017 (2018).

[21] A. V. Gritsan, J. Roskes, U. Sarica, M. Schulze, M. Xiao, and Y. Zhou, New features in the JHU generator framework: constraining Higgs boson properties from on-shell and off-shell production, Phys. Rev. D **102**, 056022 (2020).

[22] B. Bortolato, J. F. Kamenik, N. Košnik, and A. Smolkovič, Optimized probes of *CP* -odd effects in the $t\bar{t}h$ process at hadron colliders, Nucl. Phys. **B964**, 115328 (2021).

[23] R. K. Barman, D. Gonçalves, and F. Kling, Machine learning the Higgs-top *CP* phase, Phys. Rev. D **105**, 035023 (2022).

[24] J. Davis, A. V. Gritsan, L. S. M. Guerra, S. Kyriacou, J. Roskes, and M. Schulze, Constraining anomalous Higgs boson couplings to virtual photons, Phys. Rev. D **105**, 096027 (2022).

[25] A. Bhardwaj, C. Englert, R. Hankache, and A. D. Pilkington, Machine-enhanced *CP*-asymmetries in the Higgs sector, Phys. Lett. B **832**, 137246 (2022).

[26] G. Aad *et al.* (ATLAS Collaboration), Differential cross-section measurements for the electroweak production of dijets in association with a Z boson in proton–proton collisions at ATLAS, Eur. Phys. J. C **81**, 163 (2021).

[27] T. Plehn, D. L. Rainwater, and D. Zeppenfeld, Determining the Structure of Higgs Couplings at the LHC, Phys. Rev. Lett. **88**, 051801 (2002).

[28] S. Das Bakshi, J. Chakrabortty, C. Englert, M. Spannowsky, and P. Stylianou, *CP* violation at ATLAS in effective field theory, Phys. Rev. D **103**, 055008 (2021).

[29] A. Biekötter, P. Gregg, F. Krauss, and M. Schönherr, Constraining *CP* violating operators in charged and neutral triple gauge couplings, Phys. Lett. B **817**, 136311 (2021).

[30] J. Alwall, R. Frederix, S. Frixione, V. Hirschi, F. Maltoni, O. Mattelaer, H.-S. Shao, T. Stelzer, P. Torrielli, and M. Zaro, The automated computation of tree-level and next-to-leading order differential cross sections, and their matching to parton shower simulations, J. High Energy Phys. 07 (2014) 079.

[31] T. Sjostrand, S. Mrenna, and P. Z. Skands, A brief introduction to PYTHIA 8.1, Comput. Phys. Commun. **178**, 852 (2008).

[32] T. Sjöstrand, S. Ask, J. R. Christiansen, R. Corke, N. Desai, P. Ilten, S. Mrenna, S. Prestel, C. O. Rasmussen, and P. Z. Skands, An introduction to PYTHIA 8.2, Comput. Phys. Commun. **191**, 159 (2015).

[33] I. Brivio, Y. Jiang, and M. Trott, The SMEFTsim package, theory and tools, J. High Energy Phys. 12 (2017) 070.

[34] I. Brivio, SMEFTsim 3.0—a practical guide, J. High Energy Phys. 04 (2021) 073.

[35] C. Degrande, C. Duhr, B. Fuks, D. Grellscheid, O. Mattelaer, and T. Reiter, UFO—The universal FeynRules output, Comput. Phys. Commun. **183**, 1201 (2012).

[36] R. D. Ball *et al.*, Parton distributions with LHC data, Nucl. Phys. **B867**, 244 (2013).

[37] G. Aad *et al.* (ATLAS Collaboration), Modelling of the vector boson scattering process $pp \to W^{\pm}W^{\pm}jj$ in Monte Carlo generators in ATLAS, Report No. ATL-PHYS-PUB-2019-004, 2019.

[38] S. Höche, S. Mrenna, S. Payne, C. T. Preuss, and P. Skands, A study of QCD radiation in VBF Higgs production with VINCIA and PYTHIA, SciPost Phys. **12**, 010 (2022).

[39] S. Bolognesi, Y. Gao, A. V. Gritsan, K. Melnikov, M. Schulze, N. V. Tran, and A. Whitbeck, On the spin and parity of a single-produced resonance at the LHC, Phys. Rev. D **86**, 095031 (2012).

[40] A. V. Gritsan, R. Röntsch, M. Schulze, and M. Xiao, Constraining anomalous Higgs boson couplings to the heavy flavor fermions using matrix element techniques, Phys. Rev. D **94**, 055023 (2016).

[41] M. Abadi *et al.*, TensorFlow: Large-scale machine learning on heterogeneous distributed systems, arXiv:1603.04467.

[42] F. Chollet, KERAS, https://github.com/fchollet/keras, 2015.

[43] T. O'Malley, E. Bursztein, J. Long, F. Chollet, H. Jin, L. Invernizzi *et al.*, KERASTUNER, https://github.com/keras-team/keras-tuner, 2019.

[44] J. Ohnemus, Order-α_s calculations of hadronic $W^{\pm}\gamma$ and $Z\gamma$ production, Phys. Rev. D **47**, 940 (1993).

[45] U. Baur, T. Han, and J. Ohnemus, QCD corrections to hadronic $W\gamma$ production with nonstandard $WW\gamma$ couplings, Phys. Rev. D **48**, 5140 (1993).

[46] G. Aad *et al.* (ATLAS Collaboration), Observation of electroweak production of two jets and a Z-boson pair, arXiv:2004.10612.

[47] A. Tumasyan *et al.* (CMS Collaboration), Measurement of $W^{\pm}\gamma$ differential cross sections in proton-proton collisions at $\sqrt{s} = 13$ TeV and effective field theory constraints, Phys. Rev. D **105**, 052003 (2022).

[48] M. Aaboud *et al.* (ATLAS Collaboration), Observation of Electroweak Production of a Same-Sign W Boson Pair in Association with Two Jets in pp Collisions at $\sqrt{s} =$ 13 TeV with the ATLAS Detector, Phys. Rev. Lett. **123**, 161801 (2019).

[49] G. Aad *et al.* (ATLAS Collaboration), Observation of photon-induced W^+W^- production in pp collisions at $\sqrt{s} = 13$ TeV using the ATLAS detector, Phys. Lett. B **816**, 136190 (2021).

[50] G. J. Feldman and R. D. Cousins, A unified approach to the classical statistical analysis of small signals, Phys. Rev. D **57**, 3873 (1998).

[51] S. S. Wilks, The large-sample distribution of the likelihood ratio for testing composite hypotheses, Ann. Math. Stat. **9**, 60 (1938).

[52] F. Larios, M. A. Perez, G. Tavares-Velasco, and J. J. Toscano, Trilinear neutral gauge boson couplings in effective theories, Phys. Rev. D **63**, 113014 (2001).

[53] B. Grzadkowski, O. M. Ogreid, and P. Osland, *CP*-Violation in the ZZZ and ZWW vertices at e^+e^- colliders in Two-Higgs-Doublet Models, J. High Energy Phys. 05 (2016) 025.

[54] H. Bélusca-Maïto, A. Falkowski, D. Fontes, J. C. Romão, and J. a. P. Silva, *CP* violation in 2HDM and EFT: The ZZZ vertex, J. High Energy Phys. 04 (2018) 002.

[55] T. Corbett, M. J. Dolan, C. Englert, and K. Nordström, Anomalous neutral gauge boson interactions and simplified models, Phys. Rev. D **97**, 115040 (2018).

[56] A. I. Hernández-Juárez, A. Moyotl, and G. Tavares-Velasco, Contributions to ZZV^* ($V = \gamma, Z, Z'$) couplings from *CP* violating flavor changing couplings, Eur. Phys. J. C **81**, 304 (2021).

[57] ATLAS Collaboration, 10.17182/hepdata.94218.

[58] CMS Collaboration, 10.17182/hepdata.115354.